

Microfluidics Based DNA Hybridization: Mathematical Modeling issues and Future Challenges

Suman Chakraborty

Abstract | In this paper, various mathematical modeling strategies associated with the analysis of the kinetics and the transport processes pertinent to microfluidics-based DNA hybridization methodologies are critically reviewed. In particular, the coupling of specific/non-specific hybridization kinetics with the fluid flow, heat transfer and mass transfer equations is described in detail. Methodologies for obtaining faster DNA hybridization rates are also discussed and the corresponding mathematical modeling issues are identified to define the scope of ongoing and future research endeavours.

1. Introduction

1.1. The concept of DNA chips

A remarkable advancement in the technology of the micro Total Analysis Systems (μ -TAS) over the past few years has made it possible to organize and combine the processes of sample handling, analysis and detection in stand-alone integrated microfluidic platforms. This allows rapid biochemical analyses to be carried out over length scales that are several orders of magnitudes below the conventional practice. Overall, bio-microfluidics has provided great promises in improving the sensitivity, specificity and the processing time required for a sample analysis, which are the key requirements for advanced biomedical applications. In order to appreciate the significance of bio-microfluidics in advanced biomedical and biotechnological applications, it needs to be appreciated first that different methods, in principle, can be employed to detect eventual abnormalities or illnesses in patients. For viral infections or blood-related pathologies, for example, immunoassays can be performed to determine the nature of organisms that are responsible to disturb the inherent immunological defensive systems in

the living beings. One way of performing this is to use homogeneous systems in which the sample and detection molecules are both in a liquid system. Another way is to employ a heterogeneous system, in which one type of molecules involved is bound to the solid substrate. The DNA or the Deoxyribonucleic acid happens to play a critical role towards achieving this goal, in many of the related applications. As such, DNA is found within the nucleus of each cell. DNA carries the genetic information that encodes proteins and enables cell to reproduce and perform their functions. Structurally, the DNA is a linear polymer made up of repeating sub-units (monomers) known as nucleotides that are covalently bonded together. The sequence of these nucleotides forms the hereditary information. Each monomer consists of a phosphate group that is responsible for the negative charge on the DNA, a de-oxyribose sugar and a nitrogen containing base. The backbone of a single stranded DNA molecule contains a series of alternating sugar and phosphate groups, with one base attached to each sugar molecule. The double-helical DNA strands essentially contain linked nucleotides with one of the four bases adenine (A), thymine (T),

Department of
Mechanical Engineering,
Indian Institute of
Technology,
Kharagpur 721302, India
suman@mech.iitkgp.ernet.in

Electrophoresis: Electrophoresis is the movement of an electrically charged substance under the influence of an electric field. In practice, electrophoresis offers with a common method of separating large molecules (such as DNA fragments or proteins) from a mixture of similar molecules. An electric current is passed through a medium containing the mixture, and each kind of molecule travels through the medium at a different rate, depending on its electrical charge and size. Separation is based on these differences. Agarose and acrylamide gels are the media commonly used for electrophoresis of proteins and nucleic acids.

Gel Electrophoresis: Gel Electrophoresis is a technique in which components of a mixture are separated from one another on the basis of differences in charge and attraction to a gel phase. Gel electrophoresis is commonly used to separate DNA fragments based on size, yielding a unique "fingerprint". Gel electrophoresis uses positive and negative charges to separate charged particles. Electricity travels through a buffer solution in the electrophoresis chamber. The buffer allows the electric current to flow from the cathode (negative electrode) to the anode (positive electrode). DNA is negatively charged; therefore it travels toward the positive electrode.

Gene expression analysis: Gene expression analysis deals with the determination of the activity of the genes in a cell/tissue or an organism. Currently, this is mainly achieved through the determination of the mRNA quantity of specific genes, and also by the quantification of proteins.

DNA hybridization: DNA hybridization refers to the use of a segment of DNA, called a DNA probe, to identify its complementary DNA; used to detect specific genes.

guanine (G) and cytosine (C). One oxygen atom is missing in the sugar content of the nucleotide—thus the prefix “deoxy”. In the sequence of their nucleotides, and thus their bases, both strands are complementary to each other—in each case an A is opposed by a T and a G by a C; this base pairing holds it together. For genetic ailments, DNA analysis can be performed to know whether a patient possesses a mutation in a specific gene^{1–3}. One of the methods to analyze this condition is to perform a gel-phase electrophoretic separation of fragments formed from the DNA under question. Differences in fragment lengths from the patient’s DNA and a healthy reference indicate the possibilities of certain genetic ailments. Another method for accomplishing this purpose is to introduce many different known single stranded (ss) DNA sequences bound together with particles or gels in a reactive microsystem. The DNA sample under investigation can be ‘hybridized’ with these different sequences. By identifying the specific DNA sequence with which this sample reacts (note that there is only one complementary sequence with which such selective reaction becomes possible), one can determine the DNA sequence of the unknown sample. It has been well appreciated that this kind of hybridization of the DNAs to their complementary sequences plays a major role in replication, transcription and translation, where specific recognition of nucleic acid sequences by their complementary strands is essential for the propagation of information content. In practice, microchip based nucleic acid arrays presently permit the rapid analysis of genetic information by hybridization. The DNA chips have gained wide usage in bio-analytical chemistry, with applications in important areas such as gene identification, genetic expression analysis, DNA sequencing and clinical diagnostics.

1.2. *Fundamental principles of DNA hybridization*

As mentioned earlier, a general principle of operation of the heterogeneous DNA assays is to probe molecules that are bound to the solid substrates in order to detect the target molecules in a given sample. When a liquid sample is brought into contact with the substrate-bound probe molecules, the target molecules migrate towards the substrates by diffusion and react with the probe molecules. A majority of DNA microarray technologies are based on such passive nucleic acid hybridization, i.e., the binding event depends upon diffusion of target DNA molecules to the probe DNAs. Unfortunately, passive DNA hybridization approach may take several hours. This is because of the fact that the target DNAs, with a typical diffusion coefficient of the order

of 10^{-11} m²/s (for oligonucleotides that are 18 base pairs in length, for example), only reach the capture probes via Brownian (random) motion in order to hybridize⁴. Because of this diffusion-dependence, large amounts of target DNA and long hybridization times are often required to achieve detectable hybridization signals and repeatable results. As a consequence, many researchers have explored alternative methods to make the DNA sensing faster and more sensitive in solutions with low concentrations of target DNAs. One of the earlier alternative methods was to utilize electric fields to accelerate the rate of interaction between the probe and target DNA molecules, because the DNA strand has multiple negatively charged groups. In diffusion-based transport of DNA, the time (τ) it takes a DNA molecule to travel over a distance x is given as⁵

$$\tau = \frac{x^2}{2D} \quad (1)$$

where D is the diffusion coefficient. In the case of electrophoresis, the time it takes to move a molecule in the electric field over a distance x , given by⁵

$$\tau = \frac{x}{\mu_{ep}E} \quad (2)$$

where μ_{ep} is the electrophoretic mobility and E is the electric field strength. Using typical values for D (9.943×10^{-11} m²/s) and μ_{ep} (15,000 μ m²/V-s), and under an applied electric field of 0.004 V/ μ m, the electrophoretic transport may appear to be 150 times faster over a distance of 500 μ m^{5,6}. Even though fast DNA transport is distinctly advantageous in many respects, one critical disadvantage is that the sample solution containing the target DNA must be desalted before hybridization in order to establish an appropriate electric field. This is because the electric field depth exists only in close proximity to the electrodes in a solution with high salt-concentration. A high concentration of the ions nullifies the electric field in the area away from the electrodes and reduces the effective electrophoretic mobility of the DNA molecules. Therefore, to facilitate the rapid movement of DNA by an electric field, a low conductive buffer solution needs to be used. In contrast, in molecular biology, to achieve efficient hybridization, one always prefers to work with high conductivity solutions. Therefore, it is desirable to devise a DNA hybridization protocol that can deal with a wide range of buffer conductivities, and yet achieve an optimal performance. Microfluidics-based DNA hybridization holds the key towards achieving this goal in the lab-on-a-chip based microdevices of immense technological relevance.

Electric double layer: When a solid is in contact with an electrolyte, the chemical state of the surface is generally altered, either by ionization of covalently bound surface groups or by ion adsorption. As a result, the surface inherits a charge while counterions are released into the liquid. For example, common glass, SiOH, in the presence of H₂O, ionizes to produce charged surface groups SiO⁻ and release of a proton. At equilibrium, a balance between electrostatic interactions and thermal agitation generates a charge density profile. The liquid is electrically neutral, but for a charged layer adjacent to the boundary, which bears a charge locally equal in amplitude and opposite in sign to the bound charge on the surface. This charged layer is commonly known as the electric double layer (EDL).

Electroosmosis/Electroosmotic flow: Electroosmosis refers to the motion of an ionized liquid relative to a stationary charged surface by an applied electric field. In simple terms, electroosmotic flow originates from the motion of ions in a solvent environment through very narrow channels, where an electric potential gradient causes the ion migration.

1.3. DNA hybridization through microfluidics

To overcome the diffusion-controlled limits associated with passive DNA hybridization techniques, microfluidics-based DNA hybridization strategies have been proposed and implemented by a number of researchers in the recent past^{7–10}. There are several advantages associated with such microfluidic DNA arrays: these enable detection at the lowest possible DNA concentrations, allow for shorter times to achieve this detection because of enhanced mass transport, offer the ability to monitor several samples in parallel by using a multichannel approach, reduce the potential for contamination by relying on an enclosed apparatus, and hold the overall promise for integration of several functions in a single apparatus.

Various flow-actuation methodologies have been proposed by the researchers for achieving transport of the sample through the 'active' DNA hybridization chips. One of the common methods, known as electro-osmotic (EO) pumping^{11–16}, essentially relies on the mechanism of electroosmosis, which refers to the liquid flow by an applied electric field over charged liquid–solid interfaces. Fundamentally, electroosmosis can occur due to the formation of an electrical double layer (EDL) at the charged surfaces. Immobilized surface charges can develop on a solid substrate (such as the walls of a microchannel) that is in contact with an electrolyte, as a consequence of complex electro-chemical reactions. The layer of ions adsorbed and immobilized on the charged surface is called the Stern layer. Due to electrostatic and entropic interactions, the presence of such surface charges results in a re-distribution of nearby counter-ions and co-ions in the liquid phase. This leads to the formation of an EDL, so that the local charge density close to the interface is non-zero. In the diffuse layer of the EDL, the counter-ions predominate over the co-ions, so as to neutralize the net surface charge. This diffuse part of the EDL spans over a distance away from the liquid–solid interface. The characteristic order of the diffuse part of the EDL is commonly known as the Debye length. If a potential is applied along the microchannel axis, the diffuse EDL tends to move due to electrostatic interactions. Because of the cohesive nature of the hydrogen bonding of the polar solvent molecules, the entire buffer is effectively pulled along the microchannel axis, resulting in an electroosmotic flow (EOF). Such electroosmotic pumping systems work without any movable mechanical parts, and thus increase the long-term stability and reduce the difficulty of production. Furthermore, electroosmosis allows pumping of liquids over a wide range of conductivity, which is critical for most biochemical applications.

From the implementation point of view, the integration of micro or nano scale electrodes in fluidic devices is a relatively simple procedure with the advancement of MEMS-based fabrication technologies. Consequently, electrokinetic forces appear to be ideal for manipulating DNA molecules and performing fluidic operations in the pertinent biochemical systems. However, it also needs to be recognized in this context that DNA has a relatively high negative electrophoretic mobility, on account of a large number of negative charges on the molecule. Therefore, electroosmotic pumping of DNA requires a buffer with a large electroosmotic mobility so that the electroosmotic forces can overcome the negative electrophoretic mobility of the DNA molecules. Unfortunately, buffers used in DNA hybridization often contain salts in high concentrations, which reduce the electroosmotic effects to a considerable extent. In that perspective, pumping using mechanical pressure¹⁷ might possess some advantages over the electroosmotic approach in the sense that the former is insensitive to the variations in pH, macromolecular charges and the salt concentration. However, because of the huge pumping power requirements, considerable sample dispersion (associated with the parabolic-shaped characteristic velocity profiles) and the lack of precise control associated with pressure-driven microflows, mechanical pumping alone could not emerge as one of the most preferred alternatives for driving fluid flow through micro-scale conduits for DNA hybridization applications. Furthermore, because of the high back-pressures generated due to the considerable flow resistances associated with mechanically-pumped microchannel flows involving large pressure gradients, leakage prevention might itself pose a challenging operational problem, if the unit is not properly sealed. As a compromise, researchers have recently proposed¹⁸ the employment of combined electroosmotic and pressure-driven transport mechanisms, for driving DNA samples through microfluidics-based hybridization chips.

In order to impose stringent controls over the hybridization performance of these kinds of DNA-microassays without going for too many expensive and tedious in-situ experimental trials, the researchers have well recognized the needs for comprehensive mathematical modeling and detailed simulation studies on microfluidics-based DNA transport. This helps to obtain the optimal system parameters with the most favourable hybridization characteristics within the constraints of the chosen configuration. A major emphasis of the present review article, is to outline and review the various features of mathematical

modeling of DNA hybridization in the presence of combined pressure-driven and electroosmotic transport mechanisms. First, a detailed review of the various kinetics-based models of DNA hybridization will be presented. Subsequently, the coupling of the kinetics-model with the fluid flow, heat transfer and the species transport in the bulk phase are described. Some of the key results obtained by employing these considerations are highlighted. Finally, some more recently introduced methodologies of DNA hybridization and the pertinent issues of mathematical modeling are discussed.

2. DNA hybridization reaction kinetics

2.1. Basic reaction kinetics

In order to appreciate the intricacies associated with biochemical reactions in DNA hybridization microassays, it may be instructive to revisit certain basic definitions associated with the chemical kinetics of reactive systems. These basic concepts are briefly elucidated below¹⁹.

(i) *Rate of reaction*: For a chemical reaction of the form $A + nB \rightarrow mC + D$, the rate of reaction is defined as $r = r_D (= \frac{d[D]}{dt}) = \frac{1}{m} r_C (= \frac{1}{m} \frac{d[C]}{dt}) = r_A (= -\frac{d[A]}{dt}) = \frac{1}{n} r_B (= -\frac{1}{n} \frac{d[B]}{dt})$, where the expressions in the square parentheses represent the concentrations of the pertinent species in the reactive system. As such, r is a function of the concentration of individual species, i.e., $r = r([A], [B], [C], [D])$. For most substances, this relationship is of empirical in nature and needs to be fitted experimentally. The most common form of this functional relationship is $r = k[A]^a[B]^b$, where k , a , and b are time-independent coefficients. The parameter k is called the 'rate constant', which should not be confused with the thermodynamic definition of 'equilibrium constant' of a specified reaction.

(ii) *Order of reaction*: If the rate of reaction is described by the above mentioned functional form, the order of reaction is defined as: $o = a + b$. It is important to note here that the unit of k depends on the order of the reaction. For example, for a zero-order reaction k is expressed in the units of $\text{mol}/\text{m}^3/\text{s}$; for a first order reaction k is expressed in the units of $1/\text{s}$ and for a second order reaction k is expressed in the units of $\text{m}^3/\text{mol}/\text{s}$. The rate constant is usually taken to vary with the activation energy (E_a) and temperature (T) by the Arrhenius law, as $k = k_0 \exp E_a/RT$. From molecular interpretations, the rate constant is the rate of successful collisions between the reacting molecules, the activation energy represents the minimum kinetic energy of the reactant molecules in order to

form the products and k_0 corresponds to the rate at which these collisions occur.

(iii) *Adsorption and the Langmuir model*: In case of adsorption of molecules on a solid functionalized surface, there are basically three components in the reaction. There is a free substrate in the buffer fluid (often called as the target or analyte), with a concentration of $[S]$. Second, there is a surface concentration of the ligands or capturing sites immobilized on a functionalized surface, with a concentration of $[\Gamma]_0$. Finally, there is a surface concentration of the adsorbed targets (products of the reaction), with a concentration of $[\Gamma]$. The units of $[\Gamma]$ and $[\Gamma]_0$ are in mol/m^2 , whereas $[S]$ is expressed in the units of mol/m^3 . In case of adsorption, the definition of the reaction rates are somewhat modified from the usual rate constant definitions mentioned above, primarily because of the fact that the immobilization of the substrate S not only depends on the volume concentration at the wall, but also depends on the available sites for adsorption. Accordingly, one can write $-\frac{d[S]}{dt} = k_a([\Gamma]_0 - [\Gamma])[S]_w$ and $-\frac{d[\Gamma]}{dt} = k_d[\Gamma]$, where k_a and k_d are the adsorption and dissociation rates, respectively. The concentration of Γ is increased by the former and is decreased by the later, and the net rate of change is given by their balance, i.e.,

$$\frac{d[\Gamma]}{dt} = k_a([\Gamma]_0 - [\Gamma])[S]_w - k_d[\Gamma] \quad (3)$$

Equation (3) can be integrated to obtain

$$\frac{[\Gamma]}{[\Gamma]_0} = \frac{k_a[S]_w}{k_a[S]_w + k_d} [1 - \exp(-(k_a[S]_w + k_d)t)] \quad (4)$$

Eq. (4) represents an exponential growth of $[\Gamma]$ with time, till a saturation (asymptotic) value is reached ($\frac{[\Gamma]_a}{[\Gamma]_0} = \frac{k_a[S]_w}{k_a[S]_w + k_d}$ at $t = t_a$, say). After this occurs, the remaining targets or analytes may be suddenly washed out. In that case, desorption becomes the driving mechanism. With the asymptotic condition as an initial condition for the desorption reaction, the kinetics of desorption is now governed by $-\frac{d[\Gamma]}{dt} = k_d[\Gamma]$, leading to the following time variation of surface concentration:

$$\frac{[\Gamma]}{[\Gamma]_a} = 1 - k_d(t - t_a) \quad (5)$$

2.2. Kinetics of DNA hybridization

Since the molecular diffusivity of DNA fragments is typically one to three orders of magnitude smaller than the typical liquid phase diffusivity of small molecules ($\sim 10^{-9} \text{m}^2/\text{s}$), the accumulation of DNA on the target spots by surface diffusion mechanisms

is rather slow. Interestingly, despite such slow overall reaction rates, the basic reaction step leading to DNA hybridization takes place much faster²⁰. In the first phase, the probe DNA strand diffuses towards the target strand. During the subsequent collision, a so-called nucleation site is formed, involving the formation of the first short stretch of base pairing, concerning at least 3 contiguous bases. In the subsequent phase, a stable base pair may be formed during a rapid 'zippering' reaction. Otherwise, in the case of a mismatch, the nucleation site loses its stability, and the probe strand detaches and prepares for another attempt, either with the same, or with a different target strand. With the basic binding step occurring very rapidly, the overall slowness of the hybridization may be attributed to the large number of successive attempts necessary before a successful collision and/or to the limited rate of supply of the unbound probe DNA strands. Till now, it is still not very clear which one of these two potential bottlenecks forms the actual rate-limiting step for the over-all hybridization process. As such, controversies still exist on the existence of a single dominant mechanism dictating the entire DNA hybridization steps. Some researchers claim that the process is fully reaction-rate limited^{21,22}, while some others claim it to be diffusion-controlled^{23,24}. One group of researchers^{24,25} prefer to model the DNA hybridization process as a homogeneous reaction in which the target and probe strands are both suspended homogeneously in a liquid phase environment, so that one can describe the rate of reaction as

$$dH/dt = k[P - DNA][T - DNA] \quad (6)$$

where P and T refer to the probe and target DNA molecules and k is the reaction rate constant. However, other studies^{23,26} have clearly demonstrated that the heterogeneous conditions on a biochip cannot be adequately described by means of a single kinetic constant, k . These studies have revealed that the kinetic constant has a strong time-dependence, which may be expressed in the following form:

$$k = k' t^{-p} \quad (7)$$

where p is a time-dependent coefficient. For intermediate times, the value of p has been proposed as $1/2$.^{23,26}

The controversial aspects in the description of DNA hybridization rates may perhaps be attributed to the existence of widely differing time scales and disparate experimental conditions being employed to establish the theory. Intuitively, it can be expected

that on the short time scale, the binding response may be dominated by the slow binding probability. On the other hand, in the long time range, the slow diffusive DNA supply may become the rate limiting step. One of the most fundamental models of the binding kinetics on DNA biochips was presented by Chen et al.²¹. However, their model dealt with a steady-state supply of DNA probes on the target spot surface²⁰, and hence, could not capture the time-dependent effects attributed to the very slow diffusion rates of the DNA molecules. Pappaert et al.²⁷ attempted to overcome these limitations, by introducing a time-dependent diffusion transport model. To verify their model, they also conducted an extensive random walk simulation study. To determine the number of collisions per unit of time with the target spot, they adapted the classical work of Collins and Kimball²⁸ on the modeling of the kinetics of colloidal agglomeration processes. Their calculation was essentially based on the number of collisions with a surface per time and per unit surface area (N), for a collection of molecules present at a concentration C , given as²⁹

$$N = AuC \quad (8)$$

where u is the product of the mean molecular jumping frequency (ν) and the mean molecular free path (λ), and A is a dimensionless geometric constant. For the case of a pure 1-D collision process, this value can easily be shown to be given by $A = 1/2$. The number of successful collisions, n , can accordingly be obtained as

$$n\chi = 1/2 \cdot uC\chi \quad (9)$$

where χ is the binding probability. Further, for the satisfaction of the conservation of mass at the reactive boundaries, one must have, at those locations

$$n = kC \quad (10)$$

where k is given by

$$k = 1/2 \cdot \nu\lambda\chi \quad (11)$$

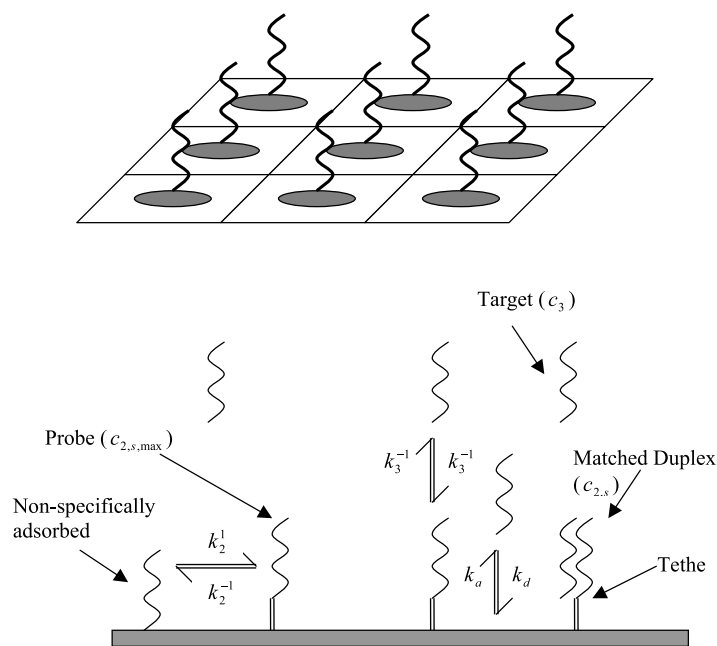
For the case of 1-D diffusion, these parameters lead to the description of a molecular diffusion coefficient, by invoking the theory of Brownian motion, as³⁰:

$$D_{mol} = \nu\lambda^2/2 \quad (12)$$

Thus, from eqs (11) and (12), one may express k as

$$k = D_{mol}\chi/\lambda \quad (13)$$

Figure 1: A schematic diagram depicting the dual mechanism of DNA hybridization



Considering the Langevin model of Brownian motion³⁰, it may also be possible to express k directly as a function of the basic physico-chemical molecular parameters. For a particle of radius of gyration R and mass m , subjected to a randomly varying external force (Brownian force) and a friction force, the mean persistence length can be described as

$$\lambda = \sqrt{\frac{k_B T m}{3\pi\mu R}} \quad (14)$$

where μ is the viscosity of the surrounding fluid, T is the absolute temperature and k_B is the Boltzmann constant. Similarly, the mean collision frequency is given as

$$\nu = \frac{3\pi\mu R}{m} \quad (15)$$

Inserting eqs (14) and (15) in eq. (22), an expression for the binding rate constant k can be obtained as a function of the basic molecular parameters such as the molecular mass, radius of gyration, etc. This analysis may also be extended to 3-D diffusion systems, by replacing the factor of 2 in eq. (12) by a factor of 6²⁰ and the factor 1/2 in eq. (11) by a factor 1/4²⁹, so that one may write

$$k = 3D_{mol}\chi/2\lambda \quad (16)$$

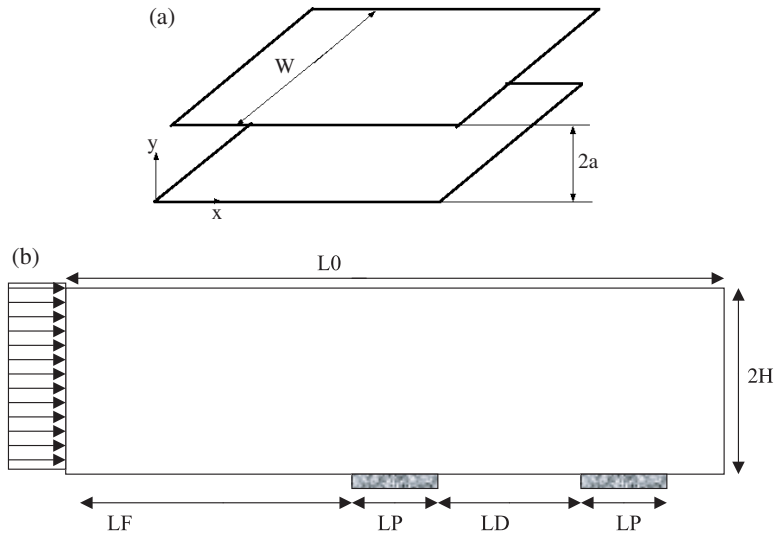
Despite being fundamentally based, a major shortcoming of the above description lies in the fact that it does not specifically relate the reaction kinetics with the detailed mechanisms of DNA hybridization. It can be noted in this context that DNA hybridization essentially occurs by means of two basic mechanisms (see fig. 1 for a schematic representation), namely, (a) a direct (specific) hybridization from the bulk phase to the surface-bound probes, and (b) an indirect (non-specific) hybridization in which the target is initially non-specifically adsorbed on the surface and then diffuses along the surface before reaching an available target probe molecule³¹. Researchers have been successful in demonstrating how the above reduction of dimensionality (RD) might enhance the overall DNA capture rate. In general, when a partner in a biomolecular reaction is immobilized on a surface, the rate of capture would depend on events in the bulk (3-D) as well as on the surface (2-D), and on the relative ratio of solute diffusion to the intrinsic reaction rate. However, hybridization that occurs in the interphase between a solid and solution is anticipated to demonstrate kinetics that are different from those observed in the bulk solution. It has been suggested in the literature²¹ that non-selective adsorption of single-stranded oligonucleotide, followed by surface diffusion (2-D diffusion coefficients) to immobilized probes can enhance hybridization rates in contrast to direct hybridization in the solution. This suggestion is based on a reduction of dimensionality of diffusion from a 3-D to a 2-D phenomenon. Exact theories in this regard, however, are yet to be well established. Nevertheless, theoretical postulates have been put forward in the literature to describe the interactions between the bulk and the surface phase kinetics mentioned as above. The reactions occurring at the probe locations can be described by the following rate equation³¹:

$$R_i = -\left(\frac{\partial c_{2,s}}{\partial t} + \frac{\partial c_{2,ns}}{\partial t}\right) \quad (17)$$

where, $c_{2,s}$ and $c_{2,ns}$ are the surface-phase concentration of specifically and non-specifically adsorbed target molecules, respectively, and $2a$. Along the non-reacting surface, the above term reduces to a zero flux boundary condition, in effect. The terms involved in equation (17) can further be expressed as a set of coupled two-dimensional kinetic equations as³¹:

$$\begin{aligned} \frac{\partial c_{2,s}}{\partial t} &= [k_3^1 c_{3,m} (c_{2,s,\max} - c_{2,s}) - k_3^{-1} c_{2,s}] \\ &+ [k_2^1 c_{2,ns} (c_{2,s,\max} - c_{2,s}) - k_2^{-1} c_{2,s}] \end{aligned} \quad (18)$$

Figure 2: (a): A schematic diagram depicting the problem domain (b): A schematic diagram depicting the probe arrangements at channel walls



and

$$\frac{\partial c_{2,ns}}{\partial t} = [k_a c_{3,m} (c_{2,ns,max} - c_{2,ns}) - k_d c_{2,ns}] - [k_2^1 c_{2,ns} (c_{2,s,max} - c_{2,s}) - k_2^{-1} c_{2,s}] \quad (19)$$

where, $c_{2,s,max}$ is the maximum concentration of the hybridized targets (equivalent to the local concentration of the surface bound probes available for hybridization), $c_{2,ns,max}$ is the maximum concentration of the non-specifically adsorbed molecules, $c_{3,m}$ is the bulk-phase concentration of the targets in surface film, k_3^1 is the kinetic association constant for direct hybridization (from solution phase), k_3^{-1} is the kinetic dissociation constant for direct hybridization (from solution phase), k_2^1 is the kinetic association constant for indirect hybridization of the non-specifically adsorbed targets (from surface phase), k_2^{-1} is the kinetic dissociation constant for indirect hybridization of the non-specifically adsorbed targets (from surface phase), k_a is the kinetic association constant for nonspecific adsorption of the targets to the surface, and k_d is the kinetic dissociation constant for nonspecific adsorption of the targets to the surface. Physically, equation (18) describes that the rate of change in surface concentration of hybridized species is a combination of the rate of change of targets getting hybridized directly from the bulk phase and the rate of targets getting hybridized after an initial non-specific adsorption. Equation (19) implies that

the rate of change in surface concentration of nonspecifically adsorbed targets is increased by the rate of adsorption from the bulk phase, but is decreased by the rate at which the non-specifically adsorbed targets become hybridized.

Determination of the kinetic constants appearing in equations (18) and (19) needs microscopic and statistical theories of collision to be essentially invoked. A physical basis of this lies in the fact that pure diffusion, with its fractal-like path, necessarily leads to an infinitely high collision rate for the situation represented here, manifested by a non-zero average solute concentration immediately in contact with each target. To account for finite reaction rates with non-zero local concentration in a diffusion-based framework, one must assume that the reaction probability per collision is diminishingly small, which may be a major deviation from the reality. The other approach, as briefly described earlier, recognizes that the molecules follow a Brownian motion path rather than a pure diffusion, which yields a finite number of collisions from a finite solute concentration near the target probe. In Brownian motion, molecular velocity has a finite persistence length, since the instantaneous momentum of the molecule can be transferred to the solvent only at a finite rate of solvent velocity. Hence, the Brownian motion persistence length plays a central role in determining both reaction kinetic rates and reduction of dimensionality enhancement. Following fundamental postulates of statistical physics²⁹ and the work of Anlerod and Wang²⁰, it can be postulated that the reaction rate of direct hybridization (R_3) can be obtained as a product of bulk-phase flux of target molecules colliding with the surface (F_3), probability of collision location being a probe site (P_p), probability that the probe is available for hybridization (P_a) and the probability that the collision will result in successful hybridization (P_r). All these effects can be combined to obtain the following equation for rate of reaction³¹:

$$R_3 = k_3^1 C_{3,m} (C_{2,ns,max} - C_{2,s}) \quad (20)$$

where $k_3^1 = \frac{3D_3 N_v \pi R_p^2 \chi_3}{2S_3}$. In equation (20), N_v is the Avogadro number, R_p is the radius of probe site, χ_3 is probability that 3-D collision will result in a successful hybridization and S_3 is frequency of collision in 3-D. A similar approach can be followed to determine the rate of reaction for non-specifically adsorbed target, as:

$$R_2 = k_2^1 C_{2,ns} (C_{2,s,max} - C_{2,s}) \quad (21)$$

where $k_2^1 = \frac{8D_2N_pR_p\chi_2}{S_2}$. In equation (21), D_2 , χ_2 and S_2 are similar to D_3 , χ_3 and S_3 , except for the fact that the earlier group represents a 2-D collision behaviour.

Although equations (20) and (21) are fundamental in nature, the reaction probability, χ_n , is rather uncertain. Instead, a classical Wetmur-Davidson relationship³² may be used to estimate the rate of hybridization for bulk-phase targets in the surface film as:

$$k_3^1 = 3.5 \times 10^5 \frac{l^{0.5}}{N} \quad (22)$$

where N is complexity of the target sequence and l is the number of nucleotide units. In general, complexity of the sequence is taken as the total number of non-repeating sequences in a DNA strand. In absence of any steric interference, in which the bulk molecules are able to move freely within the surface film, the above is likely to be valid in an approximate sense. In cases of more dense probe spacings or a large quantity of nonspecifically adsorbed targets, equation (22), however, is likely to overestimate the pertinent kinetic constant.

With the above estimation of k_3^1 , k_2^1 can be obtained by dividing equations (20) and (21), and assuming that $\chi_2 = \chi_3$, $S_2 = S_3$, as

$$k_2^1 = k_3^1 \left(\frac{16}{3\pi} \right) \left(\frac{D_2}{D_3} \right) \left(\frac{1}{R_p} \right) \quad (23)$$

The reverse kinetic constant may be obtained by appealing to thermodynamic stability requirements of the dissociation kinetics representing the solid phase hybridization reaction. Thermodynamic stability of the target probe complex is governed by Gibbs free energy of binding as

$$\frac{k^1}{k^{-1}} = \exp \left(\frac{-\Delta G}{RT} \right) \quad (24)$$

where $\Delta G = \Delta H - T\Delta S$, ΔH being the binding enthalpy and ΔS being the binding entropy. For bulk-phase hybridization, a nearest-neighbour model³³ can be used to calculate ΔG for any complementary or single-base-pair mismatched duplex. For heterogeneous hybridization, however, thermodynamic stability condition deviates from the above classical result, as the probe density is increased. Consequently, the above approximation is somewhat accurate in the limit of low probe density, with an underlying assumption that other surface effects are not thermodynamically important. Although some other thermodynamic models have been proposed in this respect³⁴, these are not

comprehensive in terms of a complete theoretical development. Instead, one may alternatively utilize equation (24), with the incorporation of Arrhenius type of formulation for k^1 and k^{-1} as

$$k^1(T) = k_0^1 \exp \left[-\frac{E_a}{R} \left(\frac{1}{T} - \frac{1}{T_0} \right) \right] \quad (25a)$$

$$k^{-1}(T) = k_0^{-1} \exp \left[-\frac{E_d}{R} \left(\frac{1}{T} - \frac{1}{T_0} \right) \right] \quad (25b)$$

where k_0^1 and k_0^{-1} are values of k^1 and k^{-1} at T_0 (T_0 is 25°C below melting temperature of DNA). Further, using $E_a - E_d = \Delta H$, k^{-1} can be estimated from the above, on estimation of either E_a or E_d (both of which are case-specific in nature). Now, since

$$k^{-1} = k_2^{-1} + k_3^{-1} \quad (26)$$

separate equations are required to estimate individual rate constants k_2^{-1} and k_3^{-1} . To achieve this goal, one may assume that at steady state an independent equilibrium exists between directly hybridized probes and targets of bulk solution, as well as between indirectly hybridized probes and nonspecifically adsorbed target molecules¹⁸. With incorporation of these into equation (18), it follows:

$$[k_3^1 c_{3,m} (c_{2,s,max} - c_{2,s,eq}) - k_3^{-1} c_{2,s,eq}] = 0 \quad (27)$$

$$[k_2^1 c_{2,ns} (c_{2,s,max} - c_{2,s,eq}) - k_2^{-1} c_{2,s,eq}] = 0 \quad (28)$$

where the subscript 'eq' represents an equilibrium state. Equations (26)–(28) can be simultaneously solved to yield k_2^{-1} , k_3^{-1} and $C_{2s,eq}$, to be used for the subsequent mathematical analysis.

Regarding nonspecific adsorption kinetics, one may note that

$$\frac{k_a}{k_d} = \frac{C_{2,n,eq}}{C_{3,m,eq} (C_{2,ns,max} - C_{2,ns,eq})} \quad (29)$$

The unknown terms appearing in right hand side of equation (29), however, are yet to be theoretically determined. Therefore, we use experimental outcomes of Chan et al.^{35,36} to estimate $C_{2,ns,eq}$, $C_{3,m,eq}$ and k_d for various types of glass substrates. The term $C_{2,ns,max}$ can be estimated by noting that because of a prior presence of surface probes (captured by specific hybridization) on target area, a full monolayer of targets cannot be adsorbed there,

Joule heating: Joule heating refers to the increase in temperature of a conductor as a result of resistance to an electrical current flowing through it. At an atomic level, Joule heating is the result of moving electrons colliding with atoms in a conductor, where upon momentum is transferred to the atom, increasing its kinetic energy.

leading to an effective radius of adsorbed target, R_t . Accordingly,

$$C_{2,ns,max} = \frac{1 - \pi R_p^2 N_v C_{2,s,max}}{N_v \pi R_t^2} \quad (30)$$

With the estimates mentioned as above, k_a can be obtained from equation (29), leading to a complete determination of kinetic constants appearing in the description of the rate of surface reaction, as given by eq. (17).

3. Continuum conservation considerations

3.1. Fundamental transport equations

Das et al.¹⁸ have recently extended the DNA hybridization model developed by Erickson et al.³¹ to include combined effects of electrokinetic and pressure-driven transport. In their study, a comprehensive mathematical model was developed, quantifying the pertinent momentum, heat and species transfer rates. Influences of bulk and surface properties on the velocity field were critically examined, which in turn dictate the nature of thermosolutal transport, and hence the DNA concentration fields, in accordance with specific and non-specific hybridization mechanisms. Joule heating³⁷ and viscous dissipation effects were also incorporated, which can cause a perceptible temperature rise, and accordingly affect various flow parameters as well as the rate constants for the hybridization.

The fundamental analysis executed by Das et al. (2006a)¹⁸ deals with the microfluidic transport through a parallel plate microchannel of height $2a$ and width w , with $w \gg 2a$ (refer to fig. 2a). Length of the channel is taken to be $L0$. Two capturing DNA probes are assumed to be attached to the bottom wall, each spanning over a length of LP (refer to fig. 2b). A potential gradient is applied along the axis of the channel, which provides the necessary driving force for electroosmotic flow. Under these conditions, an EDL forms near the liquid-wall interface. This EDL interacts with the externally applied electrical field. For example, positively charged ions of EDL are attracted towards cathode and repelled by the anode, resulting in a net body force that tends to induce bulk motion of ionized fluid in the direction of electric field. When this voltage is applied to a buffer solution with a finite thermal conductivity, the resulting current also induces an internal heat generation, often referred to as Joule heating. The thermal and fluid flow field, thus established within the channel, is responsible for the macromolecular transport, which is to be understood thoroughly to get a complete picture of the hybridization model. For mathematical modeling of the problem mentioned as above, following major assumptions are made¹⁸:

- (i) The temperature, velocity and concentration fields are unsteady and two-dimensional.
- (ii) The effect of pH change on the ensuing chemical reactions due to hydrogen and hydroxyl ions is neglected.
- (iii) The effect of charges carried by the DNA species on the electric field is neglected.
- (iv) The effect of permeation layer on the DNA transport and accumulation and electric field distribution is neglected.

The governing transport equations, under these circumstances, can be described as follows:

Continuity Equation:

$$\frac{\partial \rho}{\partial t} + \nabla \cdot (\rho \vec{V}) = 0 \quad (31)$$

X-momentum equation:

$$\frac{\partial}{\partial t} (\rho u) + \nabla \cdot (\rho \vec{V} u) = -\frac{\partial p}{\partial x} + \nabla \cdot (\mu \nabla u) + b_x \quad (32)$$

where b_x is the body force term per unit volume in x-direction, given as: $b_x = -\rho_e \frac{\partial \phi}{\partial x}$, where ρ_e is the net electric charge density and ϕ is the potential distribution due to an externally imposed electric field.

Y-momentum equation:

$$\frac{\partial}{\partial t} (\rho v) + \nabla \cdot (\rho \vec{V} v) = -\frac{\partial p}{\partial y} + \nabla \cdot (\mu \nabla v) + b_y \quad (33)$$

where b_y is the body force term per unit volume in y-direction, given as: $b_y = -\rho_e \frac{\partial \phi}{\partial y}$. In both equations (32) and (33), the dynamic viscosity, μ , is a function of temperature, given as

$$\mu = 2.761 \times 10^{-6} \exp\left(\frac{1713}{T}\right) \quad (34)$$

where T is in K and μ is in $Pa.s$. It can be noted here that the distribution of ϕ needs to be solved from the Laplace equation, as a consequence of an externally imposed electrical potential gradient. The corresponding governing differential equation is as follows:

$$\nabla \cdot (\sigma \nabla \phi) = 0 \quad (35)$$

where σ is the electrical conductivity of the solution. Further, distribution of the net electric charge density, ρ_e , appearing in the momentum

Poisson-Boltzmann equation: The Poisson-Boltzmann equation is a mathematical combination of the Poisson equation for the electrostatic potential variation and the Boltzmann distribution of ionic charges.

conservation equations, is to be ascertained by solving the Poisson–Boltzmann equation for surface potential distribution as:

$$\nabla \cdot (\varepsilon \nabla \psi) = -\frac{\rho_e}{\varepsilon_0} \quad (36)$$

where ψ denotes the electric double layer (EDL) potential, ε_0 is the permittivity of free space, and ε is the dielectric constant of the electrolyte which is a function of temperature, given as

$$\varepsilon = 305.7 \exp\left(-\frac{T}{219}\right) \quad (37)$$

where T is in Kelvin. In equation (36), ρ_e is described as:

$$\rho_e = -2n_0 e z \sinh\left(\frac{e z \psi}{k_B T}\right) \quad (38)$$

where, n_0 is the ion density (in molar units), e is the electronic charge, z is the valence, k_B is the Boltzmann constant, and T is the absolute temperature. To depict the relationship between the net electric charge density and Debye length, one may express n_0 as a function of the Debye length, λ , as

$$n_0 = \frac{\varepsilon k_B T}{8\pi e^2 z^2 \lambda^2} \quad (39)$$

Energy conservation equation:

$$\frac{\partial}{\partial t} (\rho C_p T) + \nabla \cdot (\rho C_p \vec{V} T) = \nabla \cdot (k \nabla T) + \varphi + \dot{q} \quad (40)$$

where k is the thermal conductivity of the electrolyte solution, which is a function of temperature, given as

$$k = 0.6 + 2.5 \times 10^{-5} T \quad (41)$$

where T is in K and k is in W/m².K. In equation (40), φ is the heat generation due to viscous dissipation, given as

$$\varphi = 2\mu \left[\left(\frac{\partial u}{\partial x} \right)^2 + \left(\frac{\partial v}{\partial y} \right)^2 \right] + \mu \left(\frac{\partial u}{\partial y} + \frac{\partial v}{\partial x} \right)^2 \quad (42)$$

Further, \dot{q} is the heat generation due to Joule heating, which, according to Ohm's law, can be given as

$$\dot{q} = \frac{I^2}{\sigma} \quad (43)$$

It can be noted here that the electrical current density includes two parts, one is due to the applied

electric field imposed on the conducting solution ($\sigma \vec{E}$), and the other is due to the net charge density moving with the fluid flow ($\rho_e \vec{V}$). Therefore, the electrical current density, I can expressed as

$$\vec{I} = \rho_e \vec{V} + \sigma \vec{E} \quad (44)$$

Using equations (43) and (44), one can obtain the heat generation due to Joule heating as:

$$\dot{q} = \frac{(\rho_e \vec{V} + \sigma \vec{E}) \cdot (\rho_e \vec{V} + \sigma \vec{E})}{\sigma} \quad (45)$$

Species conservation equation:

$$\frac{\partial (\rho c_i)}{\partial t} + \nabla \cdot (\rho \vec{V} c_i) = \nabla \cdot (\rho D_n \nabla c_i) + \mu_{os} z_i F \nabla \cdot (\rho c_i \nabla \phi) + \rho R_i \quad (46)$$

where, c_i is the concentration of the i^{th} species in the solution, μ_{os} is the electro-osmotic mobility of the concerned species, z_i is the valence of the i^{th} species, F is Faraday's constant. In equation (46), D_n is a generalized diffusion coefficient, which is the liquid phase diffusion coefficient (D_3) in the bulk fluid and surface phase diffusion coefficient (D_2) at the nonspecific adsorption sites. The term R_i is a generation/source term, as described by eq. (17) and as adjusted in terms of its units by dividing eq. (17) with the height of the boundary control volume.

The governing conservation equations developed here lead to a well-posed system of partial differential equations, on specification of the appropriate boundary conditions. It can be noted here that boundary conditions corresponding to DNA hybridization are already incorporated through specification of the source term R_i (equation (17)) for control volumes adjacent to the channel–fluid interface, and need not be duplicated in prescription of boundary conditions. Other pertinent boundary conditions are summarized in Table 1¹⁸.

3.2. Simplified analytical considerations

It is important to note here that the numerical computations necessary to simulate the detailed transport/hybridization model described above may be somewhat involved in nature, primarily because of the strongly interconnected and complicated features of mass, momentum and species transport characterizing the entire sequence of events. Under certain restricted conditions, however, approximate analytical solutions can also be obtained, depicting the interactions between an imposed electroosmotic flow-field and the transient DNA hybridization

Table 1: Table of boundary conditions

Governing Equation	Boundary conditions			
	Inlet ($x=0$)	Outlet ($x=L_0$)	Bottom wall ($y=0$)	Top wall ($y=2H$)
Laplace eq. (eq. 35)	$\phi = \phi_0$	$\phi = 0$	$\frac{\partial \phi}{\partial y} = 0$	$\frac{\partial \phi}{\partial y} = 0$
Poisson-Boltzmann equation (eq. 36)	$\psi = 0$	$\frac{\partial \psi}{\partial x} = 0$	$\psi = \zeta$ (zeta potential)	$\psi = \zeta$ (zeta potential)
Continuity and Momentum conservation (eq. 31–33)	$u = u_{in}$ or $\frac{\partial p}{\partial x} = K_0$ (K_0 is a constant) $v = 0$	$\frac{\partial u}{\partial x} = 0$ $v = 0$	$u = 0$ $v = 0$	$u = 0$ $v = 0$
Energy conservation (eq. 40)	$T = T_\infty$	$\frac{\partial T}{\partial x} = 0$	$T = T_w$	$T = T_w$
Species conservation equation (eq. 46)	$c_i = c_\infty$	$\frac{\partial c_i}{\partial x} = 0$	$\frac{\partial c_i}{\partial y} = 0$	$\frac{\partial c_i}{\partial y} = 0$

occurring in a microchannel. Such models can turn out to be of immense scientific appeal, in terms of having a quantitative capability of directly capturing the influences of various consequential parameters (such as fluid flow) on DNA hybridization rates, through development of close-formed expressions, without demanding more involved numerical simulations, in many cases. Keeping this in view, Das et al.³⁸ have recently obtained closed-form expressions depicting the role of flow field on DNA hybridization rates. For analytical treatment, they assumed the fluid to be of constant physical properties, and flow field to be fully developed. Furthermore, a linear bulk concentration gradient ($\frac{\partial C}{\partial x} = M$, say) was assumed to be imposed along the microchannel axis (height of the microchannel being taken as H). The concentration boundary conditions adopted in their study were as follows:

$$\text{Initial Condition: } C(0, y) = 0 \text{ for } 0 \leq y \leq H \quad (47)$$

$$\text{Boundary conditions: } \frac{\partial C(t, H)}{\partial y} = 0 \text{ for } t > 0 \quad (47a)$$

$$D \frac{\partial C(t, 0)}{\partial y} = -\frac{\partial C_H}{\partial t} \text{ for } t > 0 \quad (47b)$$

where C_H is the instantaneous surface phase concentration of the hybridized targets and D is the diffusion coefficient of single stranded DNA molecule. The relationship between C_H and the concentration in the bulk was given as

$$\frac{\partial C_H}{\partial t} = k_a (C_{H, \max} - C_H) C_{film} - k_d C_H \quad (48)$$

where k_a is the kinetic association constant for hybridization of the target with complementary probes and k_d is the kinetic dissociation constant for hybridization. In equation (48), C_{film} refers to the solution phase concentration of the DNA at the surface film, and $C_{H, \max}$ is the maximum concentration possible for the hybridized targets (which is equal to the initial concentration of the patterned probes on microchannel surface). The first term in R.H.S. of equation (48) represents second order kinetics of DNA hybridization, considering that the rate of hybridization depends on the concentration of the target oligonucleotides close to channel surface as well as the concentration of hitherto non-hybridized free probe molecules. In contrast, the kinetics of dissociation of the probe-target pair complex depends only on the concentration of hybridized species, and fairly follows first order reaction kinetics (second term in R.H.S. of equation (48)). The analytical solution for the DNA concentration distribution, as obtained from the above mentioned study, can be summarized as follows (for details of the derivation, see Das et al.³⁸):

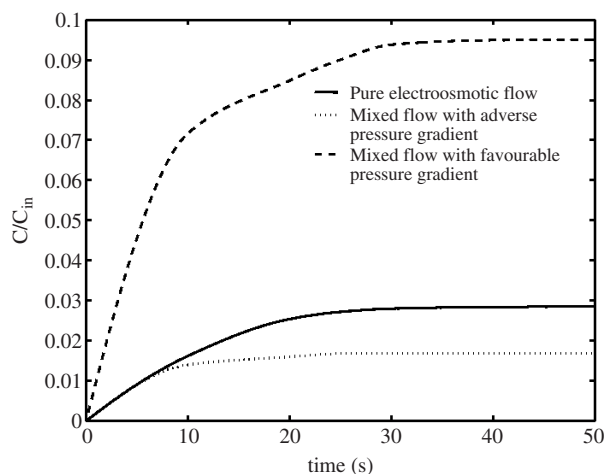
$$C(y, t) = \sum_{n=1}^{\infty} \alpha_n(t) \cos\left(\frac{n\pi y}{H}\right) - \frac{Ee^{-Ft}}{2HD} (2Hy - y^2) \quad (49)$$

In equation (49), $\alpha_n(t)$ is given as:

$$\alpha_n(t) = -\frac{2EH}{D(n\pi)^2} e^{-M_1 t} - \frac{2}{H} e^{-M_1 t} [I_1 L'_2 + I_2 M'_2 - I_3 N'_2 - I_4 P'_2 + I'_1 L'_3 + I'_2 M'_3 - I'_3 N'_3 - I'_4 P'_3] \quad (50)$$

Various parameters appearing in equations (49), (49a) are described in Appendix A.

Figure 3: Variation of concentration of hybridized targets with time, at probe location 1, for all cases. The pressure gradients taken for the computations are as follows: $\frac{\partial p}{\partial x} = -10^5$ Pa/m (favourable) and $\frac{\partial p}{\partial x} = 10^5$ Pa/m (adverse).



3.3. Numerical simulation predictions

In order to obtain significant insights regarding temporal variations of DNA concentration (hybridized targets, $c_{2,s}$) at the probes as a function of prevailing flow conditions, one may refer to fig. 3¹⁸. These simulations were carried out by employing the physical parameters and problem data enlisted in Table 2. Fig. 3, in essence, shows an initial slow rate of increment of $c_{2,s}$, followed by a comparatively higher hybridization rate that eventually approaches towards a saturation state with respect to time. It is observed that during initial transients, the concentrations of hybridized targets, for each of the cases investigated, remain somewhat close to each other. However at later instants of time, as the system approaches towards a metastable state, concentration values corresponding to different situations investigated in the above-mentioned study start differing widely from each other. For a pure electroosmotic flow, the steady value of $c_{2,s}$ is found to be somewhat less than that corresponding to a mixed flow occurring under a favourable pressure gradient, but turns out to be significantly greater than that observed for a mixed flow occurring under an adverse pressure gradient. This variation can be explained by arguing that for pure electroosmotic flows, the bulk concentration, and hence the film concentration ($c_{3,m}$), is less as compared to that established in presence of

a favourable pressure gradient, but more than that established in presence of an adverse pressure gradient. This, in turn, ensures the corresponding variations in $c_{2,s}$ values, in an analogous fashion. It has also been earlier demonstrated that the rate of the hybridization reaction can be significantly increased due to a non-specific adsorption of the single stranded DNA on the surface, and a subsequent 2-D diffusion towards surface-bound complementary probe molecules, as compared to the sole effect of 3-D hybridization from the bulk²⁰. Hence, the initial slowness of hybridization can be explained considering the 'lag time' between non-specific adsorption and consequent hybridization to the probe, mediated by two-dimensional diffusion. During this time, three-dimensional hybridization reaction dominates. However, once the lag phase is over, the rate of hybridization reaction increases at a faster pace, due to a coupled effect of the two types of mechanisms, and saturation reaction-kinetics are eventually achieved when all the single stranded probe molecules become hybridized with target complementary oligonucleotides. Regarding the specific impact of pressure gradients on DNA hybridization, it is revealed that steeper temporal gradients in concentration can be achieved with favourable pressure gradients, especially during early stages of hybridization. On the other hand, imposition of an adverse pressure gradient of similar magnitudes may not be consequential enough to retard the hybridization rates drastically. This may be attributed to the fact that although such adverse pressure gradient decelerates the flow locally, it also ensures that the target DNAs have a greater exposure time with the complementary capture probes, with an enhanced probability of hybridization. For the adverse pressure gradients reported in the above-mentioned study¹⁸, these two counteracting effects almost nullify each other, leading to relatively insignificant impacts on the resultant hybridization behaviour, especially during the early transients.

Typical cross sectional temperature distributions, as obtained from the above-mentioned study, are depicted in fig. 4(a). It is observed that the curves corresponding to adverse and favourable pressure gradients almost merge with each other. This suggests that the effect of pressure gradients (within the range of values adopted in their study) is relatively insignificant in determining the thermal field within the microchannel. This can be justified by noting that the temperature rise in the channel can be primarily attributed to Joule heating, which is solely dependent on the applied potential gradients and the electrical conductivity of the medium. An order of magnitude analysis, assessing the relative contributions of

Onsager reciprocity relationship: The Onsager reciprocal relations express the equality of certain relations between flows and forces in thermodynamic systems out of equilibrium, but where a notion of local equilibrium exists. For example, it is observed that temperature differences in a system lead to heat flows from the hotter to the colder parts of the system. Similarly, pressure differences will lead to fluid flow from high-pressure to low-pressure regions. It was observed experimentally that when both pressure and temperature vary, pressure differences can cause heat flow and temperature differences can cause matter flow. Even more surprisingly, the heat flow per unit of pressure difference and the density (matter) flow per unit of temperature difference are equal. This was shown to be necessary by Lars Onsager using statistical mechanics. Similar "reciprocal" relations occur between different pairs of forces and flows in a variety of physical systems.

Table 2: Table of physical properties and problem data

Parameter	Value
$L0$	8.5×10^{-3} m
LF	5.0×10^{-3} m
LP	1.7×10^{-4} m
LD	1.7×10^{-3} m
$2H$	$50 \mu\text{m}$
σ	10^{-3} S/m
ϵ_0	8.854×10^{-12} C/Vm
n_0	1 mol/m^3
e	1.6×10^{-19} C
ϕ_0	150 V
$u_{initial}$	2.0 m/s
ξ	-50 mV
T_w	300 K
T_∞	300 K
ρ	998 kg/m^3
k_B	1.38×10^{-23} J/K
μ_{os}	4×10^{-8} m ² /Vs
Z	20
c_{in}	1.0×10^{-6} M
$c_{3,m}$	1.9×10^{-7} M
$c_{2,s,max}$	2.0×10^{-7} mol/m ²
$c_{2,ns,max}$	1.98×10^{-7} mol/m ²
k_3^1	1×10^6 (1/Ms)
k_3^{-1}	0.49 (1/s)
k_2^1	1×10^6 m/Ms
k_2^{-1}	0.51 (1/s)
k_a	9×10^3 (1/Ms)
k_d	0.3 (1/s)
D_3	1.3×10^{-10} m ² /s
D_2	5.0×10^{-13} m ² /s

the terms $(\sigma \vec{E})$ and $(\rho_e \vec{V})$ in the expression for the net current (see Eq. 44), aptly justifies this proposition (Noting that $\left| \frac{E\vec{\sigma}}{\rho_e \vec{V}} \right| \sim O(10^5)$). Another important observation is that over typically short durations of time ($O(s)$), the temperature rise owing to Joule heating effects is virtually negligible. However, for larger time durations (fig 4b), the temperature rise becomes much more consequential, and is likely to result in significant changes in DNA transport characteristics. This interesting issue may be more critically analyzed by referring to the energy equation (Eq. 40), in which one may compare the order of magnitude of the advection and the source terms, to obtain $\Delta T \sim \frac{\sigma E_x^2 t}{\rho C_p}$, where ΔT is a characteristic temperature rise. This shows that the rise in temperature scales linearly with the operational time, all other parameters remaining unaltered. Moreover, the same scales with the square of the electric field, corresponding to a specific buffer solution and a given temporal instant. Hence, even slight increments in the electric field strength can result in significant rises in sample temperature. For transport and hybridization of macromolecules such as DNA, this rise of temperature may be of

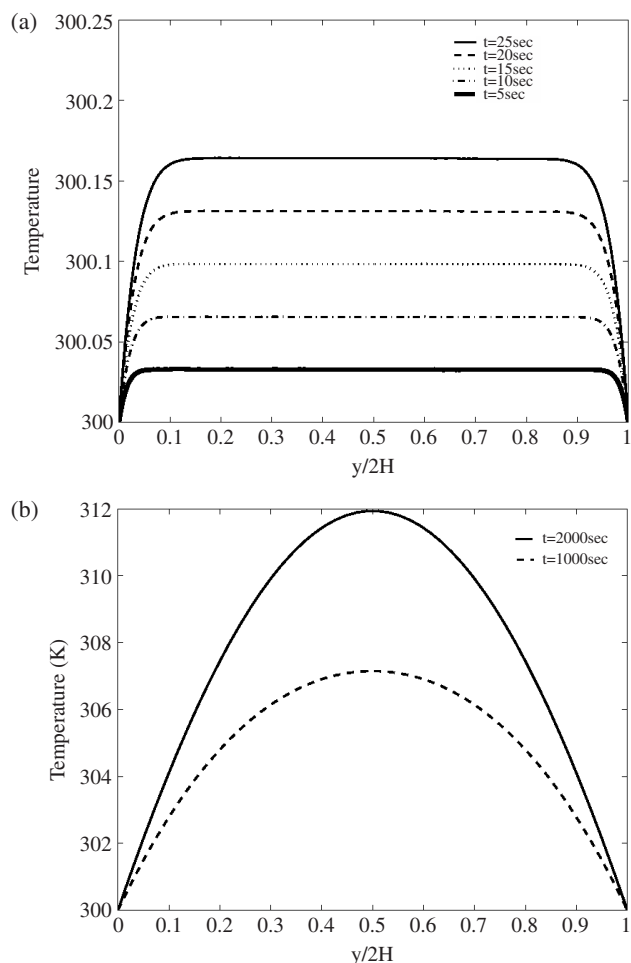
immense consequence, primarily attributable to a phenomenon called 'melting' or 'denaturation' of DNA, which is characterized by separation of the two DNA strands from an existing hybridized state. This splitting occurs at the melting temperature, T_m , defined as the temperature at which 50% of the oligonucleotides and their perfect complements are in duplex. In order to avoid problems like inappropriate duplex formation, primer mismatch etc., the hybridization is typically carried out $5^\circ-10^\circ\text{C}$ below T_m . Hence it is important that the temperature rise due to Joule heating during hybridization is not more than around 5°C . Corresponding to typical physical parameters employed in the study of Das et al.¹⁸, the order of the imposed electric field needed to be constrained within 10^5V/m , so as to ensure that the temperature rise is restricted within 5°C , thereby avoiding denaturation or melting of DNA samples. Moreover, during experimentation, it is also important to carry out the hybridization at a reasonably rapid rate, so as to ensure that the hybridized targets are saturated without incurring any further denaturation due to overheating.

4. Recent advancements and future directions

4.1. DNA hybridization by employing transverse electric fields in conjunction with surface patterning

Extending the fundamental theoretical understandings, researchers are in a continuous endeavor to obtain faster rates of DNA hybridization through the employment of a combination of several 'augmenting' mechanisms in integrated microfluidic platforms. Some of the recent findings on reactive systems with electrokinetic transport have revealed certain interesting propositions in this regard, which can be potentially exploited to obtain enhanced rates of DNA hybridization. For example, Das and Chakraborty³⁹, in a recent study, have theoretically established a novel proposition that the rate of macromolecular adsorption can be augmented with application of transverse electric fields across patterned walls of a microfluidic channel. In their study, first, an approximate fully developed velocity profile was derived, which was subsequently utilized to solve the species conservation equation pertaining to a combined advection-diffusion transport. Closed-form solutions for the concentration field were subsequently obtained, in consistency with the typical second order kinetics of macromolecular adsorption. The above-mentioned theoretical analysis has revealed that the favourable effect of transverse electric fields can be best exploited when

Figure 4: (a): Temperature profiles within the channel, at location of probe 1 (curves corresponding to both adverse and favourable pressure gradients almost merge) (b) Temperature profiles within the channel, at large time instants at location of probe 1 (curves corresponding to both adverse and favourable pressure gradients almost merge)



they are employed in conjunction with patterned microchannel surfaces. This is because of the fact that a transverse electric field, when applied across the walls of a microchannel with periodic surface patterns, may result in an additional pressure gradient in the axial direction⁴⁰, by following Onsager reciprocity relations. This effect has been subsequently utilized by us to study the enhancement in the surface adsorption of biological macromolecules³⁹, with a combination of transverse electric fields and surface patterning effects. It was theoretically demonstrated that with an externally applied favourable pressure gradient of the order of 10^5 Pa/m, along with an axial electric field of the order of 10000 V/m and a transverse electric field of the order of 1000 V/m, a DNA hybridization time of as low as 30 s could be achieved with a

pattern angle of 45° . However, comprehensive experiments need to be conducted to demonstrate the practical consequences of this theoretical proposition. Following major conclusions could be drawn from the above-mentioned study:

- (i) Benefits of transverse electric fields cannot be effectively realized if the channel surfaces are not patterned, which is primarily attributable to the excess equivalent pressure gradient that cannot be exploited without surface patterning.
- (ii) For moderate values of axial potential gradient, increase in orders of magnitude of transverse potential gradients can augment the rate of macromolecular adsorption significantly. However, a large value of the axial potential gradient may virtually suppress any contributions from an enhanced transverse electric field, and can dictate the adsorption rate by itself alone. Nevertheless, such extreme situations might be rather undesirable, because of adverse effects of Joule heating and subsequent macromolecular degradation on account of high electrical field strength. Hence, in place of a strong axial electric field, a combination of moderate values of axial and transverse electric fields can turn out to a better proposition for the practical purpose of enhancement of macromolecular transport and adsorption rates.
- (iii) The beneficial effects of transverse electric fields in terms of augmenting the rate of macromolecular adsorption can be best exploited for pattern angles in the tune of 45° . While acute angles turn out to be advantageous in this respect, in general, obtuse angles effectively slow down the rate of macromolecular transport by inducing an equivalent 'adverse' pressure gradient that retards the rate of macromolecular transport.
- (iv) In practice, a judicious combination of transverse electric fields and surface patterning effects can be employed, to augment the rate of macromolecular adsorption, without incurring any adverse implications of Joule heating and consequent macromolecular degradation on account of axial electric fields of too high a strength.

4.2. DNA hybridization by rapid micromixing

Heule and Manz⁴¹ explored the prospects of performing DNA hybridization assays in a sequential scheme, containing a split channel system for fast micromixing and a subsequent meandering channel to observe the evolution of the mixture by optical means. The problems of

limited mixing in the laminar flow regime were overcome by reducing the average diffusion distance to a few micrometers only. DNA oligomers (20-mers) of different sequences were injected on the chip for mixing. Two modes of operation were investigated. First, the samples were injected into the micromixing device at a high flow rate of 40 $\mu\text{l}/\text{min}$. The flow rate through the micromixing unit was reduced, when the sample was passed through the same, to allow for the measurement of fluorescence levels at various steady-state reaction times in the range of 2–15 s. In a buffer containing 0.2 M NaCl, 2 basepair mismatches could routinely be detected by employing this method within 5–20 s. Single base-pair mismatches were successfully identified with low salt concentrations. In the second mode, the flow was completely stopped and the evolution of the total fluorescence signal influenced by the hybridization of oligomers and photobleaching was observed. While certain technological difficulties (such as the periphery providing a steady stream of samples) still need to be addressed to ensure a successful operation of such hybridization assays in practice, this method holds the potential of providing for a very flexible and versatile platform for genomic analysis. A rigorous theoretical analysis, therefore, needs to be directed to substantiate this viewpoint.

4.3. DNA hybridization by CMOS biochips

Barbaro et al.⁴² have recently developed low-cost, portable and fully integrated solid-state biosensors for the label-free detection of DNA hybridization. This new device was realized in a standard Complementary Metal Oxide Semiconductor (CMOS) process. The detection mechanism was based on the field-effect of the intrinsic negative electric charge of DNA molecules, which modulates the threshold voltage of a floating-gate MOS transistor. A fluid cell was developed for delivering the DNA samples on the active surface of the chip. Successful measurements on first prototype of the chip, hosting 16 individually addressable sensors, were also presented as a proof of this concept. Detailed mathematical analysis need to be carried out to optimize the performance of these kinds of CMOS-based DNA chips, based on the underlying transport processes, many of which are non-trivially interlinked.

4.4. Microwave-accelerated fast DNA hybridization

Aslan et al.⁴³ designed a fast and sensitive DNA hybridization assay platform, based on microwave-accelerated metal-enhanced fluorescence (MAMEF).

In their experiments, thiolated oligonucleotide anchors were immobilized onto silver nanoparticles on a glass substrate. The hybridization of the complementary fluorescein-labeled DNA target with the surface-bound oligonucleotides could be completed within 20 s, on heating with low-power microwaves. In these studies, a significantly reduced non-specific adsorption rate was noted when using microwave heating near to silvered structures, as compared to room temperature incubation. These findings suggest that MAMEF could be a useful alternative for designing DNA hybridization assays with improved sensitivity and rapidity. Theoretical modeling efforts need to be directed to establish this proposition from a rigorous mathematical perspective, so as to impose more stringent controls on this suggested methodology.

4.5. DNA hybridization on a CD

The recent advent of CD-based microfluidics (lab-on-a-CD concept) has opened up the possibilities of implanting complicated bio-microfluidic arrangements in CD-based platforms^{44,45}. Besides being advantageous because of their versatility in handling a wide variety of sample types, the ability to gate the flow of liquids (non-mechanical valving), simple rotational motor requirements, economised fabrication methods, and large range of flow rates attainable, the possibility of performing simultaneous and identical fluidic operations makes the CD an attractive platform for multiple parallel assays. The CD platform (including the designed circuitry embedded within the same), coupled with automated liquid reagent loading systems, is ideal for a future commercial introduction of more compact and inexpensive lab-on-a-chip based bio-microfluidic systems.

The technology developed by the optical disc industry can conveniently be utilized to image the CD at the micron resolution, and possible extensions to DVD will allow submicron-scale resolution, leading to the integration of fluidics and informatics on the same disc. Moreover, the materials of the CDs are conducive for elegant microfabrication and are also extremely bio-compatible in terms of handling the DNA molecules. In a study undertaken by Jia et al.⁴⁶, an automated flow-through DNA hybridization and detection method was implemented and experimentally validated on a CD-based fluidic platform. A multilevel process utilizing SU-8 lithography was developed to obtain the fluidic structures with sufficient reagent storage volume and the desired flowrate. Thiolated-ssDNA monolayers on gold spots were used as capturing probes and biotinylated

complementary DNA was used as the target probe. Hybridization was detected for DNA samples of different concentrations down to 100 pM. The theoretical analysis presented in this regard, however, was not detailed enough to involve the solution of the kinetically-coupled transport equations. Further, from a practical viewpoint, it could also be recognized that with the aid of centrifugal forces alone, the CD-based DNA hybridization arrangements, even under the most favourable conditions, could result in hybridization times of only of the order of few minutes. This is primarily because of the fact that the centrifugal force, being a volumetric (body) force, does not scale as favourably as the surface forces over the micro-domain. However, with the additional flow-augmenting features (such as, the application of transverse and axial electric fields, surface patterning effects), an integrated and portable CD-based biomicrofluidic platform can indeed be conceptualized, with an ideal combination of fast DNA hybridization and inexpensive device fabrication. Detailed theoretical analyses in this regard, indeed, fall in the scope of future research in this area.

4.6. *Some more fundamental considerations*

In the mathematical models outlined so far, the conformational aspects of the DNA molecules have not been explicitly considered, for describing the transport and hybridization processes within the microfluidic conduits. Fundamentally, these issues can be of significant consequence for deriving more accurate DNA transport models, in the context of hybridization reactions. Although the DNA molecules resemble coils in a non-flowing state, these DNA molecules stretch and orient in the same direction in a flowing state⁴⁷. According to theoretical studies of coil–stretch transition⁴⁸, the extent of stretching and shrinking of polymer chains depends on the microchannel size, the polymer chain length, the flow speed, and the viscosity, density, and temperature of the solution. In fact, the DNA molecules change their conformation depending on the flow rates. At lower flow rates, the DNA molecules move while expanding and contracting, analogous to inchworms. On the other hand, at higher flow rates ($> 5 \mu\text{l}/\text{min}$), the DNA molecules stretch and undulate, as if they are swimming in a fluid-current. Moreover, the DNA strands became shorter in highly viscous environments and tend to become longer in higher temperature conditions, analogous to the coil–stretch transition⁴⁸ behaviour of polymer molecules. The consequences of these mechanisms, in the context of DNA hybridization, may be far from

being trivial. In fact, it has been experimentally revealed that DNA stretching in microfluidics engenders efficient hybridization of long-strand DNAs⁴⁷. In a non-extensional flow, the short DNA probes might not be able to interact with their capturing counterparts, since these DNA molecules form entangled coiled structures. In contrast, in extensional flows through microchannels, the hybridization is likely to occur more efficiently because of the promoted stretching. Control of the extent of this DNA stretch may be achieved by adjusting the solution chemistry and the flow conditions. Molecular dynamics and/or coupled continuum/molecular simulations may need to be executed to quantitatively substantiate this viewpoint. Not only that, detailed thermodynamic studies also need to be executed to establish accurate theoretical description of the variations in the free energy of the DNA molecules, while undergoing various bio-chemical reactions in the process of their hybridization. Carlon and Heim⁴⁹, in a recent study, have recently presented a thermodynamic analysis of RNA/DNA hybridization in high-density oligonucleotide microarrays. This kind of analysis, however, needs to be theoretically extended in the future to improve the parametrization of the pertinent experimental data and enhance the stability of the fitting parameters for predicting the hybridization free energies of a wide variety of DNA samples.

4.7. *Summary and Outlook*

Pressure-driven transport has conventionally been the most popular method to achieve microfluidics-based DNA hybridization. However, pressure-driven transport of biological molecules in microchannels is associated with several shortcomings, such as the loss of injected samples due to significant dispersion effects, the necessity of a substantial pumping power, and the inability to generate complex flow patterns. As an alternative, the electrokinetic flow actuating mechanisms have subsequently been proposed. The advantages with such systems are the ‘pumpless’ operation modes, minimized sample dispersion and an excellent integrability with bio-chip components. Researchers have demonstrated that such mechanisms can be employed to enhance the rate of accumulation of DNA molecules over the electrodes (saturation is achieved in as low as 2 minutes), by exploiting an interesting interplay of the dual mechanisms of 3-D and 2-D hybridization kinetics and the applied electric fields. Extending this concept, it has been theoretically established that a judicious combination of axial electric fields and favourable pressure gradients can, in principle,

reduce the hybridization time to as low as 1 minute. However, in the process, the researchers could also realize that one can only employ limited strengths of the axial electric fields in practice, so as to avoid the adverse consequences of the Joule heating effects associated with the conductive transport of ionic charges in a fluidic medium. In fact, in order to avoid denaturation/melting of hybridized DNA samples, one can only employ an axial electric field that does not permit any rise of temperature beyond approximately 5°C.

Researchers have also independently attempted to employ transverse electric fields instead of the axial ones, for favorably exploiting the electrophoretic migration of the charged DNA molecules towards the capturing probes. As ongoing and future endeavors, the researchers might seek a judicious combination of the axial and the transverse electric fields, so as to exploit a favorable coupling of the effects of the convective DNA transport and the electrophoretic DNA accumulation. In particular, one may be interested to obtain the optimal combinations of the axial and the transverse electric fields that can give the fastest possible DNA hybridization out of the chosen configuration, without violating the Joule heating constraints. Theoretical research has shown that with such arrangements, one could possibly reduce the DNA hybridization time from minutes to seconds. There are several other microfluidic issues that also need to be addressed to exploit the possibilities of achieving much faster DNA hybridization rates. These include the variations in flow rate, channel height, inlet buffer composition, DNA concentration, surface patterning effects in conjunction with transverse electric fields, centrifugal effects etc. Typical flow rates that are currently being employed for DNA hybridization through pressure-driven flows are in the tunes if 10 $\mu\text{L}/\text{min}$ ^{17,50}. On the other hand, recent theoretical investigations¹⁸ have revealed that the plug-like velocity profiles associated with the electroosmotic transport might require a flow rate as small as 0.10 $\mu\text{L}/\text{min}$, to achieve identical hybridization rates.

With a combination of various hybridization-augmenting mechanisms, one could, in principle, achieve the same task of DNA hybridization with the nominal flow rates lowered even further. It is important to recognize in this context that this kind of lowering of the desired flow rates is also associated with the requirement of lower sample volumes, for a given sensitivity of the diagnostic device. Not only that, it has been comprehensively revealed that for a low concentration of target DNA samples, lower volumetric flow rates favor the DNA hybridization

efficiency^{17,50}. Thus, flow rate control appears to be an essential aspect of designing faster DNA hybridization microarrays. Selection of an optimum channel height is also critical in ensuring the best possible rate of DNA hybridization. This is because of the fact that over different length scales, disparate physical features might play the governing role in controlling the transport and the hybridization mechanisms. For example, when the channel height is of the order of 10–100 μm , decreasing the channel height significantly enhances the DNA hybridization. However, research investigations have revealed that below a threshold channel height (typically, of the order of 1 μm), the electric double layer formed at the channel walls can significantly protrude into bulk, thereby causing a significant dispersion in the electroosmotic flow profile. As a result, the transport and hybridization mechanisms could be significantly hindered. It has also been well-demonstrated in the literature that increases in the bulk concentration may lead to higher concentrations of the target DNA molecules close to the capturing probes, thereby augmenting the rate of DNA hybridization^{17,50,51}, for example, used a bulk concentration of 0.4 μM , so as to achieve DNA hybridization rates of the order of a few minutes.

While it is well understood that a more concentrated DNA solution is expected to have faster hybridization characteristics, an indefinite increase in the bulk concentration of the target DNA molecules is also not advisable. This is because of the fact that beyond a critical concentration limit (depending on the channel dimensions and flow characteristics), the rheological behaviour of the microflow might get significantly altered, with strongly-hindered solutal transport characteristics. Moreover, in a recent theoretical investigation⁵², it has been demonstrated that a non-uniform wall zeta potential, created by employing localized transverse electric fields, can augment DNA hybridization rates, with an optimal concentration of the inlet buffer. A characteristic hybridization time of around 45 seconds could be estimated from the theoretical analysis, for a buffer pH of 4. Since the buffer composition essentially dictates the effective macromolecular charge⁵³, its diffusion coefficient⁵⁴, and its electrophoretic mobility, an optimal choice of the inlet buffer composition may result in the most favourable hybridization characteristics; all other conditions remaining unaltered. However, insufficient quantitative information is available in the reported literature to conclusively establish this proposition.

Preliminary theoretical analysis has also revealed that the favourable effect of transverse electric fields

can be best exploited when they are employed in conjunction with patterned microchannel surfaces. This is because of the fact that a transverse electric field, when applied across the walls of a microchannel with periodic surface patterns, may result in an additional pressure gradient in the axial direction, by following Onsager reciprocity relations. This effect has been utilized by researchers³⁹ to study the enhancement in the surface adsorption of biological macromolecules, with a combination of transverse electric fields and surface patterning effects. It has been theoretically demonstrated in the above work that with an externally applied favourable pressure gradient of the order of 10^5 Pa/m, along with an axial electric field of the order of 10000 V/m and a transverse electric field of the order of 1000 V/m, a DNA hybridization time of as low as 30s could be achieved with a pattern angle of 45° . However, more detailed studies need to be conducted to demonstrate the practical consequences of this theoretical proposition. Additionally, one may utilize the centrifugal forces involved in the rotation of CDs in the transport and subsequent hybridization of DNA molecules in microfluidic channels⁴⁶, so as to exploit the pertinent techno-commercial advantages mentioned as earlier.

One may attempt to utilize optimal combinations of various actuating mechanisms and the critical system parameters to achieve a faster yet inexpensive methodology of DNA hybridization than the state-of-the-art affairs, and practically implement the same through the design and fabrication of novel bio-microfluidic devices. To achieve this purpose, one needs to investigate a wide variety of parameters and configurations, so as to come up with a practically-implementable and relatively inexpensive optimal methodology for fast DNA hybridization. Fundamental studies on the mathematical description of the underlying fluid dynamic and bio-chemical transport mechanisms, indeed, are likely to play vital roles towards achieving this goal, without attempting for too many 'hit-and-miss' type of expensive experimental trials. More extensive and detailed simulation studies, therefore, need to be executed to map the variations in the microfluidic system parameters/configurations with the DNA hybridization rates, for a wide range of practical conditions in order to come up with the most optimal solution.

Acknowledgements

The author gratefully acknowledges the financial support provided by the NSF, USA, for the Project titled "JRES: U.S.-India Fast DNA Hybridization in Microfluidic Platforms", the financial support provided by the DST, Govt. of India for the project titled "Experimental and Theoretical Studies on DNA Hybridization in Microchannels with Electrokinetically driven Flow", and the financial grants provided by the Indo-US Science and Technology Forum for the Project titled "Indo-US Center on Futuristic Manufacturing", for doing this work. The author is also grateful to the principal foreign collaborator of his research group, Prof. M. J. Madou (University of California, Irvine), for his valuable comments and active support. Finally, the author also acknowledges the contributions of his two doctoral students, Siddhartha Das and Tamal Das, for their valuable work related to microfluidics based DNA hybridization.

Appendix A: Description of parameters appearing in equations (49), (49a)

$$\begin{aligned}
 I_1 &= \frac{H}{n\pi} \left[\sin\left(\frac{n\pi}{2}\right) \right] \\
 I_2 &= \frac{H}{n\pi} \left[\frac{H}{2} \sin\left(\frac{n\pi}{2}\right) - \frac{H}{n\pi} \right] \\
 I_3 &= \frac{H^3}{n\pi} \sin\left(\frac{n\pi}{2}\right) \left[\frac{1}{4} - \frac{2}{(n\pi)^2} \right] \\
 I_4 &= \frac{H}{n\pi \left(1 + \left(\frac{H}{n\pi\lambda}\right)^2\right)} \left[e^{-\frac{H}{\lambda}} \sin\left(\frac{n\pi}{2}\right) + \frac{H}{n\pi\lambda} \right] \\
 I'_1 &= -\frac{H}{n\pi} \sin\left(\frac{n\pi}{2}\right) \\
 I'_2 &= \frac{H^2}{n\pi} \left[\frac{\cos(n\pi)}{n\pi} - \frac{1}{2} \sin\left(\frac{n\pi}{2}\right) \right] \\
 I'_3 &= -\frac{H^3}{4n\pi} \sin\left(\frac{n\pi}{2}\right) + \frac{2H^3}{(n\pi)^2} \cos(n\pi) + 2\left(\frac{H}{n\pi}\right)^3 \sin\left(\frac{n\pi}{2}\right) \\
 I'_4 &= \frac{H}{n\pi \left(1 + \left(\frac{H}{n\pi\lambda}\right)^2\right)} \left[\frac{H}{n\pi\lambda} e^{\frac{H}{\lambda}} \cos(n\pi) - e^{-\frac{H}{\lambda}} \sin\left(\frac{n\pi}{2}\right) \right] \\
 L'_2 &= \frac{Mu_{HS}}{M_1} [e^{M_1 t} - 1] + \frac{E}{H(M_1 - F)} [e^{(M_1 - F)t} - 1] \\
 M'_2 &= \frac{EF}{D(M_1 - F)} [e^{(M_1 - F)t} - 1] - \frac{Mu_{HS}}{M_1\lambda} e^{-\frac{H}{\lambda}} [e^{M_1 t} - 1] \\
 N'_2 &= \frac{EF}{2HD(M_1 - F)} [e^{(M_1 - F)t} - 1] \\
 P'_2 &= \frac{M}{M_1 u_{HS}} [e^{M_1 t} - 1] \\
 L'_3 &= \frac{Mu_{HS} - \frac{H}{\lambda} e^{-\frac{H}{\lambda}} Mu_{HS}}{M_1} [e^{M_1 t} - 1] + \frac{E}{H(M_1 - F)} [e^{(M_1 - F)t} - 1] \\
 M'_3 &= \frac{EF}{D(M_1 - F)} [e^{(M_1 - F)t} - 1] + \frac{Mu_{HS}}{M_1\lambda} e^{-\frac{H}{\lambda}} [e^{M_1 t} - 1] \\
 N'_3 &= \frac{EF}{2HD(M_1 - F)} [e^{(M_1 - F)t} - 1] \\
 P'_3 &= \frac{M}{M_1 u_{HS}} [e^{M_1 t} - 1]
 \end{aligned}$$

with $M_1 = \left(\frac{n\pi}{\lambda}\right)^2$.

Received 28 November 2006; revised 25 January 2007.

References

- Schena M., Shalon D., Davis R.W., Brown, P.O., Quantitative monitoring of gene expression patterns with a complementary DNA microarray, *Science* 270, 467–470 (1995)
- Brown P., Botstein D., Exploring the new world of the genome with DNA microarrays. *Nature Genetics* 21(1 Suppl), 33–37 (1999)
- Bier F.F., Kleinjung F., Scheller F.W., Real time measurement of nucleic acid hybridization using evanescent wave sensors—steps towards the genosensor. *Sensors and Actuators B* 38, 78–82 (1997)
- Nkodo A.E., Garnier J.M., Tinland B., Ren H., Desruisseaux C., McCormick L.C., Drouin G., Slater G.W., Diffusion coefficient of DNA molecules during free solution electrophoresis, *Electrophoresis* 22, 2424–2432 (2001)
- Kassegne S. K., Resse H., Hodko D., Yang J. M., Sarkar K., Smolko D., Swanson P., Raymond D. E., Heller M. J., Madou M. J., Numerical modeling of transport and accumulation of DNA on electronically active biochips, *Sensors and Actuators B* 94, 81–98 (2003)
- Heller M.J., Forster A.H., Tu E., Active microelectronic chip devices which utilize controlled electrophoretic fields for multiplex DNA hybridization and other genomic applications, *Electrophoresis* 21, 157–164 (2000)
- Fan Z.H., Mangru S., Granzow R., Heaney P., Ho W., Dong Q., Kumar R., Dynamic DNA hybridization on a chip using paramagnetic beads, *Anal. Chem.* 71, 4851–4859 (1999)

8. Benoit V., Steel A., Torres M., Lu Y.Y., Yang H.J., Cooper J., Evaluation of three-dimensional microchannel glass biochips for multiplexed nucleic acid fluorescence hybridization assays, *Anal. Chem.* 73, 2412–2420 (2001)
9. Adey N.B., Lei M., Howard M.T., Jenson J.D., Mayo D.A., Butel D.L., Coffin S.C., Moyer T.C., Hancock A.M., Eisenhoffer G.T., Dalley B.K., Mcneely M.R., Gains in sensitivity with a device that mixes microarray hybridization solution in a 25- μ m-thick chamber, *Anal. Chem.* 74, 6413–6417 (2002)
10. Wang Y., Vaidya B., Farquar H.D., Stryjewski W., Hammer R.P., Mccarley R.L., Soper S.A., Microarrays assembled in microfluidic chips fabricated from poly(methyl methacrylate) for the detection of low-abundant DNA mutations, *Anal. Chem.* 75, 1130–1140 (2003)
11. Woolley T., Hadley D., Landre P., deMello A.J., Mathies R.A., Northrup M.A., Functional integration of PCR amplification and capillary electrophoresis in a microfabricated DNA analysis device, *Anal. Chem.* 68 (1996) 4081–4086.
12. Waters C., Jacobson S.C., Kroutchinina N., Khandurina J., Foote R.S., Ramsey J.M., Microchip device for cell lysis, multiplex PCR amplification, and electrophoretic sizing, *Anal. Chem.* 70, 158–162 (1998).
13. Hadd A.G., Raymond D.E., Halliwell J.W., Jacobson S.C., Ramsey J.M., Microchip device for performing enzyme assays, *Anal. Chem.* 69, 3407–3412 (1997)
14. Chiem N., Harrison D.J., Microchip-based capillary electrophoresis for immunoassays: analysis of monoclonal antibodies and theophylline, *Anal. Chem.* 69, 373–378 (1997).
15. SalimiMoosavi H., Tang T., Harrison D.J., Electroosmotic pumping of organic solvents and reagents in microfabricated reactor chips, *J. Am. Chem. Soc.* 119, 8716–8717 (1997)
16. Das S., Chakraborty S., Analytical Solutions for velocity, temperature and concentration distribution in electroosmotic microchannel flows of a non-Newtonianbio-fluid, *Analytica Chimica Acta* 559, 15–24 (2006a)
17. Kim J. H-S., Marafie A., Jia X-Y, Zoval J. V., Madou M. J., Characterization of DNA hybridization kinetics in a microfluidic flow channel, *Sensors and Actuators B* 113, 281–289 (2006a)
18. Das S., Das T., Chakraborty S., Modeling of coupled momentum, heat and solute Transport during DNA hybridization in a microchannel in presence of electroosmotic effects and axial pressure gradients, *Microfluidics and Nanofluidics* 2, 37–49 (2006a)
19. Berthier J., Silberzan P., *Microfluidics for Biotechnology*, Artech House, Boston, USA (2005)
20. Axelrod D., Wang M. D., Reduction-of-dimensionality kinetics at reaction-limited cell surface receptors, *Biophys J* 66, 588–600 (1994)
21. Chan V., Graves D. J., McKenzie S. E., The biophysics of DNA hybridization with immobilized oligonucleotide probes, *Biophys J* 69, 2243–2255 (1995)
22. Jensen K.K., Orum H., Nielsen P.E., Norden B., Kinetics for hybridization of peptide nucleic acids (PNA) with DNA and RNA studied with the BIAcore technique, *Biochemistry* 36, 5072–5077 (1997)
23. Vontel S., Ramakrishnan A., Sadana A., An evaluation of hybridization kinetics in biosensors using a single-fractal analysis. *Biotechnology and Applied Biochemistry* 31, 161–170 (2000)
24. Christensen U., Jacobsen N., Rajwanshi V. K., Wengel J., Koch T., Stopped-Aow kinetics of locked nucleic acid (LNA)-oligonucleotide duplex formation: studies of LNA-DNA and DNA-DNA interactions, *Biochemical Journal* 354, 481–484 (2001)
25. Stillman B.A., Tonkinson J.L., Expression microarray hybridization kinetics depend on length of the immobilized DNA but are independent of immobilization substrate. *Analytical Biochemistry* 295, 149–157 (2001)
26. Sadana A., Vo-Dinh T., Single- and dual-fractal analysis of hybridization binding kinetics: Biosensor applications, *Biotechnology Progress* 14, 782–790 (1998)
27. Pappaert K., Van Hummelen P., Vanderhoeven J., Baron G.V., Desmet G., Diffusion–reaction modelling of DNA hybridization kinetics on biochips, *Chemical Engineering Science* 58, 4921–4930 (2003)
28. Collins F.C., Kimball, G. E., Diffusion-controlled reaction rates. *Journal of Colloid Science* 4, 425–437 (1949)
29. Reif F., *Fundamentals of Statistical and Thermal Physics*. McGraw–Hill, New York (1984)
30. Berry R.S., Rice S.A., Ross J., *Physical Chemistry*. New York: Wiley (1980)
31. Erickson D., Li D., Krull U. J., Dynamic Modeling of DNA Hybridization Kinetics for Spatially Resolved Biochips, *Analytical Biochemistry* 317, 186–200 (2003)
32. Wetmur J. G., Davidson N., Kinetics of renaturation of DNA, *J Mol Biol* 31, 349–370 (1968)
33. SantaLucia J. Jr., Allawi H. T., Seneviratne P. A., Improved nearest-neighbor parameters for predicting dna duplex stability, *Biochemistry* 35, 3555–3562 (1996)
34. Vainrub A., Pettitt B. M., Thermodynamics of association to molecule immobilized in an electric double layer, *Chem Phys Lett* 323,160–166 (2000)
35. Chan V., Graves D., Fortina P., McKenzie S. E., Adsorption and surface diffusion of DNA oligonucleotides at liquid/solid interfaces, *Langmuir* 13, 320–329 (1997)
36. Chan V., McKenzie S. E., Surrey S., Fortina P., Graves D. J., Effect of hydrophobicity and electrostatics on adsorption and surface diffusion of DNA oligonucleotides at liquid/solid interfaces, *J Colloid Int. Sci.* 203,197–207(1998)
37. Chakraborty, S., Analytical Solutions of Nusselt number for Thermally Fully Developed Flow in Microtubes under a combined action of Electroosmotic forces and imposed Pressure Gradients, *International Journal of Heat and Mass Transfer.* 49, 810–813 (2006)
38. Das S., Das T., Chakraborty S., Analytical solutions for rate of DNA hybridization in a microchannel in presence of pressure-driven and electroosmotic flows, *Sensors and Actuators B* 114, 957–963 (2006b)
39. Das S., Chakraborty S., Augmentation of macromolecular adsorption rates through transverse electric fields generated across patterned walls of a microfluidic channel, *Journal of Applied Physics* 100, 014098 (2006b)
40. Ajdari, A., Transverse electrokinetic and microfluidic effects in micropatterned channels: Lubrication analysis for slab geometries, *Phys. Rev. E* 65, 016301 (2001)
41. Heule M., Manz A., Sequential DNA hybridisation assays by fast micromixing, *Lab Chip* 4, 506–511 (2004)
42. Barbaro M., Bonfiglio A., Raffo L., Alessandrini A., Facci P., Bar'ak I., Fully electronic DNA hybridization detection by a standard CMOS biochip, *Sensors and Actuators B* 118, 41–46 (2006)
43. Aslan K., Malyn S. N., Geddes C. D., Fast and sensitive DNA hybridization assays using microwave-accelerated metal-enhanced fluorescence, *Biochemical and Biophysical Research Communications* 348, 612–617 (2006)
44. Zoval J.V., Madou M.J., Centrifuge-based fluidic platforms, *Proc. IEEE* 92, 140–153 (2004)
45. Madou M., Zoval J., Jia G., Kido H., Kim J., Kim N., Lab on a CD, *Annual Review of Biomedical Engineering* 8, 601–628 (2006)
46. Jia G., Ma K-S, Kim J., Zoval J. V., Peytavi R., Bergeron M. G., Madou M. J., Dynamic automated DNA hybridization on a CD (compact disc) fluidic platform, *Sensors and Actuators B* 114, 173–181 (2006)
47. Yamashita K., Yamaguchi Y., Miyazaki M., Nakamura H., Shimizu H., Maeda H., Direct observation of long-strand DNA conformational changing in microchannel flow and microfluidic hybridization assay, *Analytical Biochemistry* 332, 274–279 (2004)

48. DeGennes P.G., Coil–stretch transition of dilute flexible polymers under ultra-high velocity gradients, *J. Chem. Phys.* 12, 5030–5042 (1974)
49. Carlon E., Heim T., Thermodynamics of RNA/DNA hybridization in high-density oligonucleotide microarrays, *Physica A* 362, 433–449 (2006)
50. Kim D., Tamiya E., Kwon Y., Development of a novel DNA detection system for real-time detection of DNA hybridization, *Current Applied Physics* 6, 669–674 (2006b)
51. Okahata Y., Kawase M., Niikura K., Ohtake F., Furusawa H., Ebara Y., Kinetic measurements of DNA hybridization on an oligonucleotide-immobilized 27-mhz quartz crystal microbalance, *Anal Chem.* 70, 1288–1296 (1998)
52. Das S., Chakraborty S., Manuscript Under Consideration (2006c)
53. Carré A., Lacarrière V., Birch W., Molecular interactions between DNA and an aminated glass substrate, *J. Colloid Int. Sci.* 260, 49–55 (2003)
54. Chen Z., Chauhan A., DNA separation by EFFF in a microchannel, *J. Colloid Int. Sci.* 285, 834–844 (2005)



Suman Chakraborty (age 32 years) is currently an Assistant Professor at the Indian Institute of Technology (IIT), Kharagpur, India. He obtained his Ph.D from the Indian Institute of Science (IISc), Bangalore in the year 2002. His current areas of research include Transport phenomena in phase change processes, Computational fluid dynamics, and Microfluidics/ microscale transport processes. He is the recipient of INSA medal for Young Scientist, INAE Young Engineering Award, Alexander von-Humboldt Fellowship, best International CFD Thesis Award and he is a chosen member of the Indo-Japan and Indo-US teams of his area of expertise. At present, he is an author of 74 International Journal papers and the principal investigator of 5 sponsored (R&D/Consultancy) Projects.